Revisit Active Power Oscillation in Multi-Virtual Synchronous Generators Grid

Xiao, J.; Bauer, P.; Qin, Zian

DOI
10.1109/APEC48143.2025.10977432

Publication date
2025

Document Version
Final published version

Published in
APEC 2025 - 14th Annual IEEE Applied Power Electronics Conference and Exposition

Revisit Active Power Oscillation in Multi-Virtual Synchronous Generators Grid

Junjie Xiao
Electrical Sustainable Energy
Delft University of Technology
Delft, The Netherlands
J.Xiao-2@tudelft.nl

Pavol Bauer
Electrical Sustainable Energy
Delft University of Technology
Delft, The Netherlands
P.Bauer@tudelft.nl

Zian Qin
Electrical Sustainable Energy
Delft University of Technology
Delft, The Netherlands
Z.Qin-2@tudelft.nl

2025 IEEE Applied Power Electronics Conference and Exposition (APEC) | 979-8-3315-1611-6/25/$31.00 ©2025 IEEE | DOI: 10.1109/APEC48143.2025.10977432

***Abstract*—Active power oscillation (APO) issues may arise during the deployment of multiple parallel converters with Virtual Synchronous Generator (VSG) control in Microgrids. To that end, the equivalent circuit models of a converter with VSG control are proposed, which intuitively reveals the root cause of APOs. Accordingly, a graph-theory-based virtual impedance is introduced to harmonize parameters among involved VSGs, effectively eliminating APOs. Simulation and experimental results verify the improvements of the proposed control.**

***Index Terms*—Power oscillation, distributed control, damping control, virtual synchronous generator.**

I. Introduction

THE distributed generation (DG) technology has received widespread attention. The transition from droop control to VSG control for DG control can enhance critical frequency indicators such as the rate of change of frequency (RoCoF), thereby benefiting grid stability [1]. However, introducing oscillatory dynamics complicates the system, potentially leading to significant active power oscillations. These oscillations occur when multiple VSGs operate in stand-alone (SA) mode [2]. The large instantaneous currents associated with these oscillations can trigger overcurrent protection mechanisms, exacerbating system stability issues [3], [4]

Various variants of VSG control have been proposed to suppress oscillations. They can be broadly classified into two main categories: model-free and model-based approaches. For instance, the model-free approach, such as [5], [6], detects frequency deviations from its nominal and assigns different inertia at different phases. Specifically, larger inertia is applied to counteract these deviations when the DG frequency deviates from the common frequency. In contrast, smaller inertia accelerates convergence when DG frequencies align with the common frequency. This method ensures that all DG frequencies promptly synchronize with the common frequency. Furthermore, [7] proposes a self-adaptive inertia and damping combination control method to enhance frequency stability through an interleaving control technique. In short, these adaptive methods introduce a nonlinear element into DG operation, potentially altering the carefully designed inertia.

Another philosophy incorporates an extra feedback loop into the original VSG. For instance, in [8], deviations between a DG's frequency and the system's common frequency are detected, leading to adjustments of the DG. Studies in [9], [10] integrate variations in a DG's power, frequency, or phase during transients to establish feedback loops. These feedback loops fed the oscillation element into the VSG decision process, achieving disturbance compensation. Moreover, by utilizing low-bandwidth communication, the graph theory-based secondary frequency control can achieve the frequency consensus under SA mode [11]–[13]. In [14], [15], frequency disparities with neighboring DGs are employed to develop a mutual damping term. Despite the technical effectiveness of these model-free methods, they become effective only after oscillations occur and have been detected.

In addition to model-free methods, model-based approaches are employed to mitigate APO. For instance, [16] adjusts the damping and inertia coefficients simultaneously to determine and maintain the optimal damping ratio, thereby suppressing power and frequency oscillations throughout the operation. Similarly, [17] proposes an additional damping correction loop that adjusts the system damping ratio without affecting the steady-state frequency droop characteristic. However, this approach changes the preset inertial response of the VSG. In [18], the active power reference is feedforward to compensate for the VSG frequency to enhance damping. However, this feedforward controller is designed explicitly for changes in power reference, so it does not mitigate power allocation in SA mode. Moreover, [19] analyzes the power oscillation mechanism and utilizes virtual impedance to suppress power oscillations caused by line mismatches. In [20], parameter design principles are defined to eliminate all transient circulating power theoretically. [21] utilizes a phase feedforward path to replace the traditional frequency compensation path; this can enhance the damping. Nevertheless, an ideal parameter necessitates full knowledge of the system. Although these model-based methods provide effective damping for oscillation mitigation, they typically require foreknowledge of the system, such as feeder impedance. This cannot be assured in practical scenarios.

Another gap is that the existing models explaining the APO issues induced by the VSG transfer function are overly complicated and absent physical meaning. This article proposes an intuitive modeling perspective for VSG oscillation analysts, which visualizes the VSG control loop as a circuit element

with resistance, inductance, and capacitance and considers the load switch as a current source. Moreover, this paper offers suggestions for suppressing the APO in multiple VSG systems.

This paper's main contributions are summarized as follows:

1) The VSG equivalent circuit model is proposed, which provides clear physical interpretations. In this model, inertia, damping, and feeder impedance are analogized to capacitance, resistance, and inductance, respectively. Load switches are excitation sources injecting power into the circuit. The power oscillations are viewed as LC resonance phenomena.

2) A distributed virtual impedance method is proposed to attenuate oscillations in the SA mode. It benefits faster response to load variations and less communication dependence.

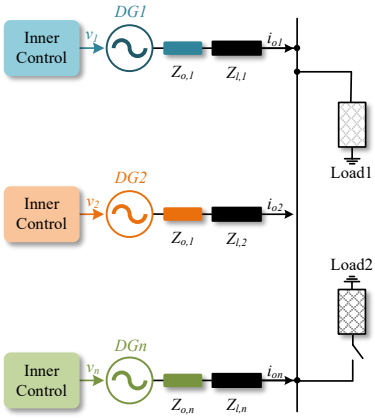

Fig. 1: The microgrid configuration consisting of n DGs.

II. Revisit VSG Control

This section reviews the two most discussed primary controls among n-distributed generators-tied microgrids, as shown in Fig.1, where the inverter can be modeled as a voltage in series with an output impedance $Z_{o,i}$ and feeder impedance $Z_{l,i}$ of i-th inverter. Herein, $Z_{l,g}$ is the grid impedance. This paper assumes feeder impedance is predominantly inductive.

A. Review on Traditional Droop and VSG Control

The power control loops of droop and VSG control are shown in Fig.2. The difference between VSG and droop control mainly focuses on the active power control loops, and the reactive power loops are ignored.

The active power loop for droop control is shown in (1).

$$\omega = \omega_0 - m_p \frac{\omega_c}{s+\omega_c}(P - P_r) \tag{1}$$

where ω represents the generated angular frequency reference of the inverter output voltage, ω_0 is the nominal value of angular frequency, m_p is the droop coefficient, P represents the inverter output active power, P_r is the nominal value of active power, m_p is the droop coefficient, and ω_c is the cutoff angular frequency of the low-pass filter.

The active power control equation for VSG is shown in (2).

$$P_r - m_g(\omega - \omega_0) - P - k_d(\omega - \omega_0) = M\frac{d(\omega - \omega_0)}{dt} \tag{2}$$

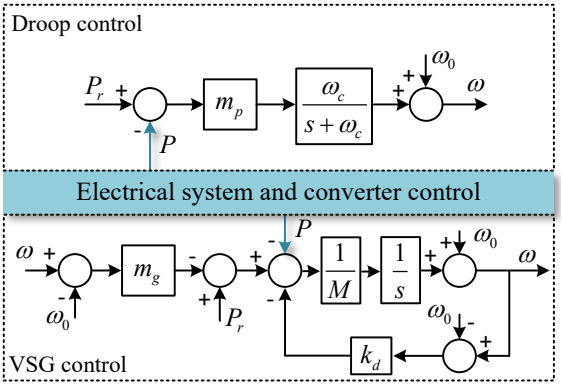

Fig. 2: Active power loop implementation

where m_g is the proportional coefficient of the governor, k_d is the damping factor, and M is the moment of inertia.

Accordingly, the small-signal model of droop control and VSG is simplified, as shown in Fig.3 and Fig.4, respectively.

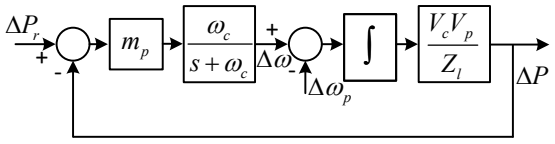

Fig. 3: Small-signal model of droop control.

In Fig.3, ω_p is the angular frequency of the point of common coupling (PCC). V_c represents the unit output voltage, V_p is the PCC voltage, and Z_l denotes the feeder impedance, ω_p is the PCC frequency disturbance. In the following, $K = V_c V_p / Z_l$.

Considering the RoCoF requirements, the dynamic performance of angular frequency when the load changes is the main focus in the SA mode. For droop control, the small-signal transfer function of angular frequency change $\Delta\omega$ over loading transition ΔP is shown in (3).

$$G_{d,sa} = \frac{\Delta\omega}{\Delta P} = -m_p \frac{\omega_c}{s+\omega_c} = -m_p \frac{1}{s/\omega_c + 1} \tag{3}$$

By simplifying the inertial and damping term in Fig.2 with $J = M$ and $D = k_d + m_g$. The small signal model of VSG in Fig.2 can be simplified as shown in Fig.4.

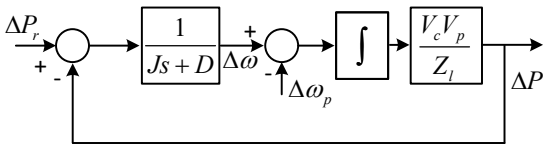

Fig. 4: Small-signal model of VSG control.

The transfer function of VSG control in stand-alone mode is shown in (4), respectively.

$$G_{v,sa} = \frac{\Delta\omega}{\Delta P} = -\frac{1}{Js+D} = -\frac{1}{D}\frac{1}{Js/D+1} \tag{4}$$

Combining (3)-(4), with $m_p = 1/D$, $\omega_c = D/J$, the droop control can be equivalent to VSG control. In this paper, the VSG is adopted for the power converter control verification.

B. Active Power Oscillation with VSG control

As VSG simulates the synchronous generator's inertia and damping characteristics, the oscillation characteristics are inevitably introduced. This subsection investigates the mechanism of active power oscillation in SA mode.

The active power across the feeder is shown in (5).

$$P_i = \frac{V_i V_p}{Z_i} sin\delta_i = K_i \frac{\Delta\omega_i - \Delta\omega_p}{s} \tag{5}$$

where δ_i is the power angle difference of the i-th converter and the PCC power angle. Within a multi-unit system, the coupling of different units is caused by PCC frequency variation.

Based on the small signal diagram of VSG, the transfer function from the PCC voltage fluctuates to i-th VSG output variation characteristics can be expressed as (6):

$$\begin{cases} \Delta P_i = \dfrac{-K_i(J_i s + D_i)}{J_i s^2 + D_i s + K_i} \Delta\omega_p \\ \Delta\omega_i = \dfrac{K_i}{J_i s^2 + D_i s + K_i} \Delta\omega_p \end{cases} \tag{6}$$

The output power of the involved DGs is equal to the load power P_L, which can be represented as in (7).

$$\sum_{i=1}^{n} \Delta P_i = \Delta P_L \tag{7}$$

By combining equations (6)-(7), the transfer function that describes the interaction between load changes and PCC frequency variations for VSGs under SA mode can be derived as shown in (8). This derivation facilitates calculating the PCC frequency responses of VSGs under varying load conditions.

$$\Delta\omega_p = -\frac{1}{\sum_{i=1}^{n} G_i(s)(J_i s + D)} \Delta P_L \tag{8}$$

where $G_i = -K_i/(J_i s^2 + D_i s + K_i)$. For a multi-VSG scenario, the load change causes a variation in PCC frequency. As shown in (6), the different transfer functions from PCC frequency to DG's outputs lead to a DG's dynamic disparity, which contributes to the oscillations. By combining equations (6)-(8), the transfer function describes the dynamics and steady state of the DGs when the load switch is shown as in (9).

$$\begin{cases} \Delta\omega_i = -\dfrac{G_i(s)}{\sum_{k=1}^{n} G_k(s)(J_k s + D)} \Delta P_L \\ \Delta P_i = -\dfrac{G_i(s)(J_i s + D)}{\sum_{k=1}^{n} G_k(s)(J_k s + D)} \Delta P_L \end{cases} \tag{9}$$

Based on the analysis above, increasing the damping coefficient D or decreasing the inertia coefficient J within a certain range can suppress active power and frequency oscillations in multi-VSG systems during load changes. However, since D is coupled with the droop coefficient, representing the steady-state frequency deviation, modifying D will inevitably change the frequency deviation nadir. Additionally, decreasing J is undesirable for VSGs as it may violate the RoCoF rules. Consequently, a trade-off between the dynamic and steady-state performance of the VSG is unavoidable. Moreover, existing virtual impedance techniques may be ineffective, as exact parameter matching of parallel VSGs may not be fully achievable. While inserting substantial virtual impedance into the control loop can mitigate oscillations, it also leads to considerable and unexpected voltage drops.

III. Equivalent Impedance Circuit of VSG

An equivalent circuit model is developed in this section to understand the root cause of APO issues intuitively, which ultimately leads to mitigation measures.

A. Single-VSG Equivalent

From the VSG small signal in Fig.4, the following equation can be rephrased as in (10) and (11):

$$\frac{1}{K_i}\frac{d\Delta P_i}{dt} = \Delta\omega_i - \Delta\omega_p \tag{10}$$

$$\Delta P_{ri} = \Delta P_i + J_i \frac{\Delta\omega_i}{dt} + D_i \Delta\omega_i \tag{11}$$

Tab.I shows the analogy relationships between the control and circuit variables. where subscript i represents the DGi's parameter, while subscript g represents those of the utility grid, and subscript p represents the PCC's parameter.

TABLE I: Correspondence between VSG and circuit variables

circuit	U_i	U_p	I_i	I_{ri}	I_L	R_i	C_i	L_i	L_g
VSG	$\Delta\omega_i$	$\Delta\omega_p$	ΔP_i	ΔP_{ri}	ΔP_L	$1/D_i$	J_i	$1/K_i$	$1/K_g$

With the analogy, ω_i is equivalent to the voltage U_i, representing the frequency change. ΔP_i is the equivalent to the current I_i, representing the active power change. J_i is equivalent to a capacitance C_i, is the inertia coefficient; $1/D_i$ is the resistance R_i, is the damping factor; $1/K_i$ is equivalent to an inductance L_i, representing feeder impedance term. According to Tab.I, (10) and (11), the VSG model can be equivalent to the circuit model, as shown in (12) and (13).

$$L_i \frac{dI_i}{dt} = U_i - U_p \tag{12}$$

$$I_{ri} = I_i + C_i \frac{dU_i}{dt} + \frac{U_i}{R_i} \tag{13}$$

As shown in (7), the current should follow $\sum_{i=1}^{n} I_i = I_L$.

Combining (6)(7) and (12)(13), the VSG model can be analogized to the circuit in Fig.5. Accordingly, the $P-f$ relationship in the VSG is analogous to the $I-V$ relationship in a second-order RLC circuit. The inertia coefficient J_i suppresses frequency changes similarly to how the capacitor stabilizes circuit voltage. The damping coefficient D_i governs

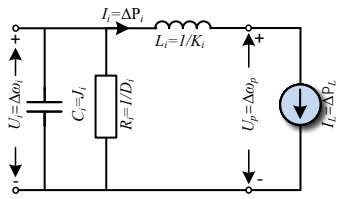

Fig. 5: Single VSG equivalent circuit.

the angular frequency changes in output power, analogous to how resistance determines the voltage change in the circuit.

The current source I_L is enabled when the load switches. Consequently, the current I_i increases to I_L. The capacitance C_i reduces the voltage change rate U_i, analogying that VSG provides inertia and maintains RoCoF. The steady-state U_i is determined by R_i, which acts as the droop coefficient that dictates the frequency deviation. As the comparison in Section II, a key distinction between droop and VSG control is the inclusion of capacitance in the latter.

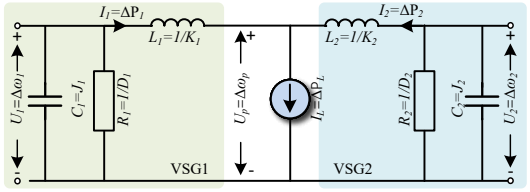

Fig. 6: Multi-VSG's equivalent circuit perspective in SA mode

B. Multi-VSG Equivalent

In this section, the transient of a multi-VSG system under SA mode is intuitively analyzed through the resonance in its equivalent impedance circuits. Subsequently, the resonance in the equivalent circuit can be quantitatively analyzed, providing insights for deriving circuit parameter configuration rules. Similarly, VSG parameters can be configured to eliminate power oscillations during the VSG's transient.

Based on Fig.5, the multi-VSG equivalent circuit can be derived. In this section, a two-VSG system is considered, for example, and can be expanded to a n VSG system. They can be equivalent to the impedance circuit perspective as shown in Fig.6. The interaction $I_1 + I_2 = I_L$ holds throughout the entire operation. This indicates that the circuit operates in parallel, and the current sharing ratio I_1:I_2 is determined by the equivalent impedance of each branch, where the impedance Z_{ei} is shown in (14).

$$Z_{ei} = \frac{U_p}{I_i} = -\frac{1}{C_i s + R_i} - sL_i \tag{14}$$

With a given current source, the current I_i is determined by the impedance, where the resonance may occur and the resonance inconsistency leads to disproportional current sharing. Herein, the circuit current I_i sharing analysis includes: 1) steady-state current sharing and 2) dynamic current sharing. The steady-state current sharing is characterized by the proportional setting of the resistors R_i, consistent with the damping coefficients D_i. Moreover, accurate dynamic current sharing means no current oscillation is within the system. This requires that the circuit model's impedance Z_{ei} remains proportional throughout the dynamic process.

Accordingly, the circuit elements should be tuned proportionally to avoid oscillation. Converting to the VSG control variable in Tab.I, the VSG parameters should be set as in (15). Here, P_{mi} denotes the maximum output active power capacity of i-th converter.

$$\frac{P_{mi}}{P_{mj}} = \frac{J_i}{J_j} = \frac{D_i}{D_j} = \frac{K_i}{K_j} = \frac{Z_j}{Z_i} \tag{15}$$

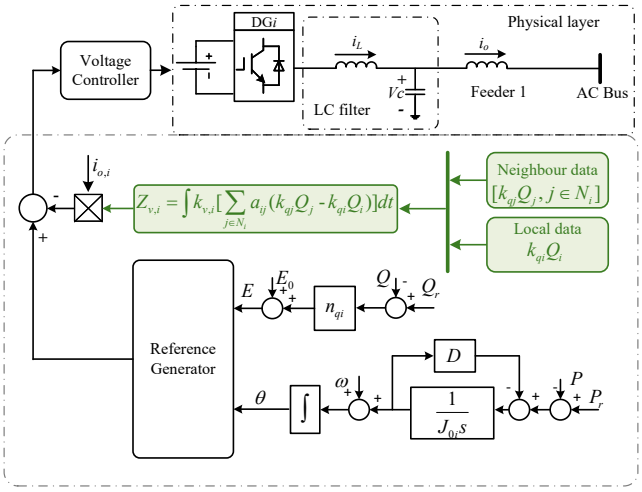

Fig. 7: Control structure of the proposed method.

IV. Proposed Control Design

With the parameter design method proposed in Section III, the transient circulating current in a multi-VSG system can be theoretically eliminated. While the inertia and damping settings can be satisfied by configuring J to maintain the same ratio as D across multiple VSGs, achieving the ideal impedance ratio is often impractical due to uncertainties in actual line inductances. To address this limitation, this section derives a new VSG control strategy based on a n-VSG system. The oscillations can be mitigated by suitably harmonizing the virtual impedance, thereby tuning the equivalent impedance. Analogizing to the circuit model in Fig.6, the inductance L_i is tunned, while the capacitance C_i and resistance R_i can be set properly by the DG's output capacity ratio.

Accordingly, mismatched equivalent output impedance can lead to uneven reactive power sharing. This indicates that the equivalent impedance has been well adjusted when the reactive power is proportionally distributed. This adjustment can help mitigate active power oscillations when the load is switched.

As the feeder is assumed to be inductive, the power flowing through the feeder impedance results in a voltage drop ΔV_i, which can be expressed as:

$$\Delta V_i \approx \frac{X_{e,i} Q_i}{V_{c,i}} \tag{16}$$

where $X_{e,i}$ is the equivalent impedance of i-th VSG. In [22]–[24], it is demonstrated that proper design of the virtual impedance enables modification of the equivalent feeder impedance $X_{e,i}$. This adjustment, in turn, facilitates control of the voltage drop among the units, thereby promoting proportional sharing of reactive power.

1) Communication network modelling: The microgrid's communication network is represented using an undirected cyber graph [25], illustrating how converters exchange information with neighboring units. Each VSG communicates with its adjacent VSGs through the communication network. It can be described by the communication adjacency matrix $A = (a_{ij})_{N\times N}$. The entry a_{ij} is set to 1 if units i and j are regularly communicating, and 0 otherwise. The degree of vertex ζ_i is defined as $d_i = \sum_{j=1}^{N} a_{ij}$. The corresponding degree matrix is $D_M = \text{diag}(d_1, \ldots, d_N)$. The Laplacian matrix L of the communication network is defined as $L = D_M - A$.

2) Graph Theory-Based Virtual Impedance implementation: The proposed method is shown in Fig.7. The inverters exchange information related to reactive power $(Q_1/D_1, \ldots, Q_N/D_i)$ with their adjacent units to achieve a reactive power consensus when the impedance has been appropriately adjusted. The reshaped consensus algorithm-based virtual fundamental impedance is expressed as (17).

$$Z_{v,i} = \int k_{v,i}[\sum_{j\in N_i} a_{ij}(Q_j/D_j - Q_i/D_i)]dt \qquad (17)$$

where the parameter $k_{v,i}$ determines the bandwidth of the virtual impedance loop, which should be slower than that of the reactive power loop. The reactive power calculation typically includes a low-pass filter, which sets the speed of the reactive power calculation. The upper bound of $k_{v,i}$ is constrained by the bandwidth of this low-pass filter, while the lower bound is dictated by the minimum required speed for virtual impedance adjustments. The adaptively adjusted impedance $Z_{v,i}$ is influenced by neighboring information and the local unit's state. When reactive power is improperly allocated, the consensus algorithm prompts the controller to adjust the virtual impedance. This modification aims to achieve balanced reactive power distribution, ensuring proportional sharing across equivalent impedance.

V. Verification

The proposed strategy has been tested in Simulink to validate its effectiveness, where three inverters connected in parallel are considered. In this microgrid system, the output side of the inverters is connected to the AC bus through an LC filter and line impedance. The expected active power-sharing ratio is assumed to be 1:2:3. In this paper, a ROCOF threshold of 1 rad/s^2 is assumed, as it falls within the typical range of minimum and maximum values reported in [26]. However, this threshold may be adjusted based on practical requirements. The verification parameters for both simulation and experiments are shown in Tab.II.

TABLE II: Parameters for Verification

Symbol	Description	Value 1
U_{dc}	DC voltage	300V
f_s	Switch frequency	20kHz
Z_L	Feeder impedance	2.2mH
L_f	Inductor of LC filter	2.2mH
C_f	Capacitor of LC filter	12μF
ω_0	Nominal angular frequency	314rad/s
V_0	Nominal voltage amplitude	150V
$k_{v,i}$	Virtual Impedance loop gain	0.01

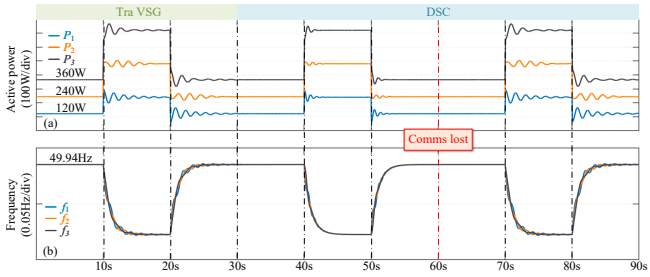

Fig. 8: Dynamics with the distributed secondary control in [12]

A. Simulation Result

Fig.1 shows the simulation structure. Herein, J_1=D_1=300, J_2=D_2=600, J_3=D_3=900. The simulation illustrates the effectiveness of the proposed method over the traditional VDG and the method in [12] under SA mode.

Fig.8 compares traditional VSG control, and the distributed secondary control proposed in [12]. The output active power and frequency are displayed in Figure 8(a) and Figure 8(b), respectively. Initially, the conventional VSG control is used to regulate the microgrids, resulting in a proportional steady-state active power-sharing ratio of 1:2:3. At 10 seconds, a 700W load is added, which, leads to decreased frequency. However, the active power and frequency experience oscillations due to the mismatched feeder impedance. When the load is suddenly switched off, the system recovers to its original power level, but oscillations persist in the dynamics. At 30 seconds, the distributed secondary control (DSC) proposed in [12] is activated, providing extra damping for the VSG system. As seen at 40 and 50 seconds, where the load is stepped on and off, the oscillations are relatively smaller than the conventional VSG control. Since DSC necessitates a communication network,

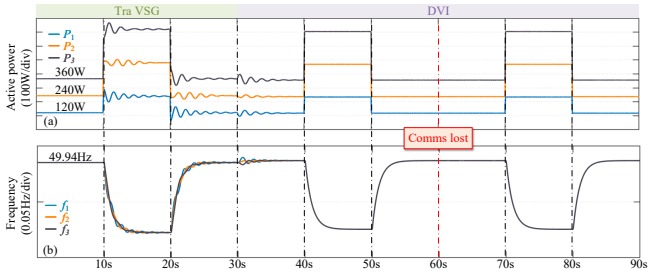

Fig. 9: Dynamics with the proposed distributed virtual impedance

it is reasonable to consider the scenario of communication loss. At 60 seconds, the communication is removed, indicating that the inverters can no longer receive information from each other. In this case, when the load increases and decreases at 70 and 80 seconds, respectively, the active power and frequency oscillations are equivalent to those observed under traditional VSG control, indicating that DSC loses its effectiveness in mitigating oscillations. This demonstrates that DSC is not robust against communication disruptions.

Fig.9 compares the proposed distributed virtual impedance (DVI) control and the conventional VSG control. Similarly, the load increases and decreases at 10 s and 20 s, respectively, leading to active power and frequency oscillations. At 30 seconds, the distributed virtual impedance control is activated. While a slight oscillation occurs due to the tuned impedance affecting the active power slightly, the system demonstrates improved stability. When the load is switched at 40 and 50 seconds, the active power and frequency smoothly transition to their steady state without significant oscillations. This illustrates the effectiveness of the proposed DVI control method. At 60 seconds, the communication is removed. The DVI has been fixed and will not be changed anymore. Therefore, the parameters can remain matched for the rest of the operation. Consequently, even with load changes at 70 and 90 seconds under the no-communication scenario, the active power and frequency do not experience oscillations. This procedure suggests that the proposed DVI control method is more immune to communication delays and interruptions than the DSC.

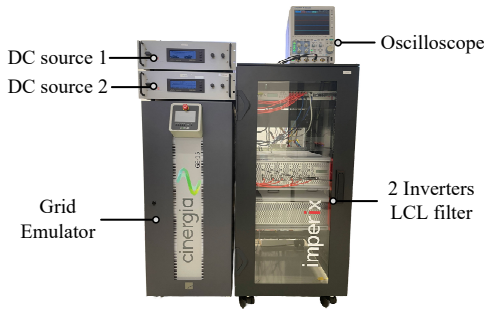

Fig. 10: Experiment setup.

B. Experiment Result

The proposed adaptive control strategy has also been validated through experiments, which involved two VSG-based inverters and an ideal grid emulator. The experimental setup is illustrated in Fig.10. In this setup, the parameters are set as $J_1 = D_1 = 100$ and $J_2 = D_2 = 200$.

This study's experimental results for active power, frequency, and reactive power are depicted in Fig.11. The system initially undergoes a loading phase followed by an unloading phase. The results demonstrate that significant oscillations between all sources are evident in the output active power and frequency when conventional VSG control is employed. This is accompanied by disproportionate sharing of reactive power. Notably, poor frequency dynamic performance, such as significant frequency overshoot, poses a risk of unexpected load-shedding or extensive blackouts.

Fig.12 illustrates the effectiveness of the proposed DVI method in mitigating active power oscillations. Following system development and subsequent DVI activation, dynamic adjustments of the reactive power are observed. These adjustments result in the reactive power Q_1 and Q_2 approaching their expected values, ultimately achieving a ratio of 1:2. As discussed in the previous section, appropriate reactive power sharing implies that the equivalent impedance of the DGs has been proportionally tunned. When inertia and damping coefficients are proportionally set following the DGs' maximum output capacity and RoCoF requirements, all parameters are harmonized, thereby eliminating the oscillations caused by VSG control. This is evident in Fig.12, where post-DVI activation, load variations do not induce oscillations. Furthermore, with DVI, the frequency change rate remains as expected.

VI. Conclusion

The VSG control can be revisited from an impedance circuit perspective, where VSG oscillations are analogous to LC resonance for an Intuitive understanding of the power oscillations issue. A distributed virtual impedance is proposed to harmonize the parameters and attenuate oscillations in SA mode to address these oscillations. The application of the proposed method yields several benefits: 1) The VSG control and its oscillations can be understood in a more intuitive way. 2) power oscillations can be precisely and quickly attenuated without requiring prior knowledge of the feeder impedance.

Acknowledgement

ECS4DRES is supported by the Chips Joint Undertaking under grant agreement number 101139790 and its members, including the top-up funding by Germany, Italy, Slovakia, Spain, and The Netherlands.

References

[1] X. Meng, J. Liu, and Z. Liu, "A generalized droop control for grid-supporting inverter based on comparison between traditional droop control and virtual synchronous generator control," *IEEE Transactions on Power Electronics*, vol. 34, no. 6, pp. 5416–5438, 2019.

[2] Q.-C. Zhong and G. Weiss, "Synchronverters: Inverters that mimic synchronous generators," *IEEE Transactions on Industrial Electronics*, vol. 58, no. 4, pp. 1259–1267, 2011.

[3] S. Chen, Y. Sun, H. Han, Z. Luo, G. Shi, L. Yuan, and J. M. Guerrero, "Active power oscillation suppression and dynamic performance improvement for multi-vsg grids based on consensus control via coi frequency," *International Journal of Electrical Power & Energy Systems*, vol. 147, p. 108796, 2023.

[4] J. Zhu, C. D. Booth, G. P. Adam, A. J. Roscoe, and C. G. Bright, "Inertia emulation control strategy for vsc-hvdc transmission systems," *IEEE transactions on power systems*, vol. 28, no. 2, pp. 1277–1287, 2012.

[5] X. Hou, Y. Sun, X. Zhang, J. Lu, P. Wang, and J. M. Guerrero, "Improvement of frequency regulation in vsg-based ac microgrid via adaptive virtual inertia," *IEEE Transactions on Power Electronics*, vol. 35, no. 2, pp. 1589–1602, 2020.

[6] M. Li, W. Huang, N. Tai, L. Yang, D. Duan, and Z. Ma, "A dual-adaptivity inertia control strategy for virtual synchronous generator," *IEEE Transactions on Power Systems*, vol. 35, no. 1, pp. 594–604, 2020.

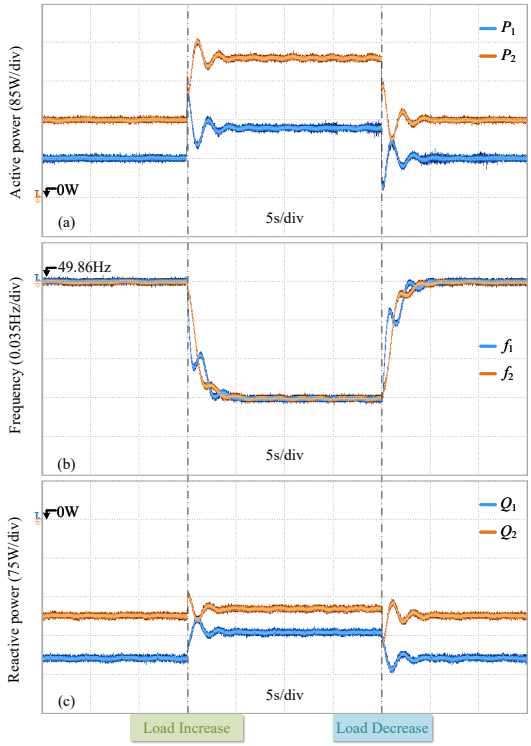

Fig. 11: Dynamic of the VSG control in SA mode

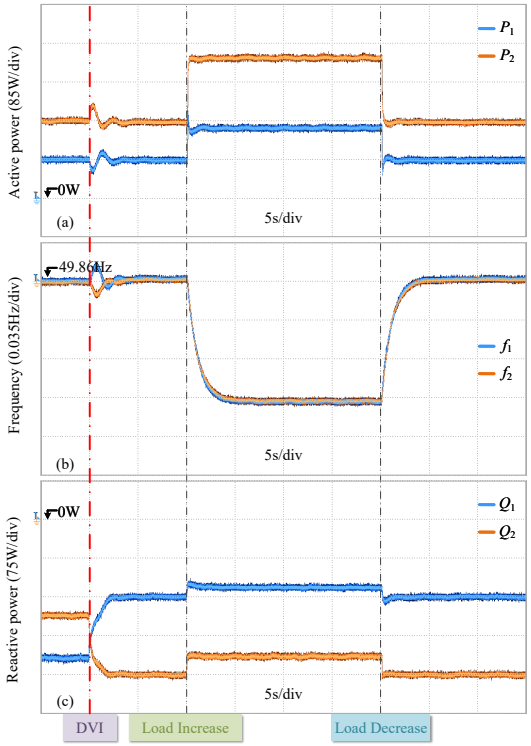

Fig. 12: Dynamic of the proposed control in SA mode.

[7] D. Li, Q. Zhu, S. Lin, and X. Y. Bian, "A self-adaptive inertia and damping combination control of vsg to support frequency stability," *IEEE Transactions on Energy Conversion*, vol. 32, no. 1, pp. 397–398, 2017.

[8] L. Li, Y. Sun, Y. Liu, P. Tian, and S. Shen, "A communication-free adaptive virtual inertia control of cascaded-type vsgs for power oscillation suppression," *International Journal of Electrical Power & Energy Systems*, vol. 149, p. 109034, 2023.

[9] M. Chen, D. Zhou, and F. Blaabjerg, "Active power oscillation damping based on acceleration control in paralleled virtual synchronous generators system," *IEEE Transactions on Power Electronics*, vol. 36, no. 8, pp. 9501–9510, 2021.

[10] Z. Wang, Y. Chen, X. Li, Y. Xu, C. Luo, Q. Li, and Y. He, "Active power oscillation suppression based on decentralized transient damping control for parallel virtual synchronous generators," *IEEE Transactions on Smart Grid*, vol. 14, no. 4, pp. 2582–2592, 2023.

[11] S. Fu, Y. Sun, L. Li, Z. Liu, H. Han, and M. Su, "Power oscillation suppression in multi-vsg grid by adaptive virtual impedance control," *IEEE Systems Journal*, vol. 16, no. 3, pp. 4744–4755, 2022.

[12] M. Shi, X. Chen, J. Zhou, Y. Chen, J. Wen, and H. He, "Frequency restoration and oscillation damping of distributed vsgs in microgrid with low bandwidth communication," *IEEE Transactions on Smart Grid*, vol. 12, no. 2, pp. 1011–1021, 2021.

[13] J. Xiao, L. Wang, Z. Qin, and P. Bauer, "A resilience enhanced secondary control for ac micro-grids," *IEEE Transactions on Smart Grid*, vol. 15, no. 1, pp. 810–820, 2023.

[14] X. Gao, D. Zhou, A. Anvari-Moghaddam, and F. Blaabjerg, "An adaptive control strategy with a mutual damping term for paralleled virtual synchronous generators system," *Sustainable Energy, Grids and Networks*, vol. 38, p. 101308, 2024.

[15] Y. Yu, S. K. Chaudhary, G. D. A. Tinajero, L. Xu, J. C. Vasquez, and J. M. Guerrero, "Active damping for dynamic improvement of multiple grid-tied virtual synchronous generators," *IEEE Transactions on Industrial Electronics*, vol. 71, no. 4, pp. 3673–3683, 2024.

[16] F. Wang, L. Zhang, X. Feng, and H. Guo, "An adaptive control strategy for virtual synchronous generator," *IEEE Transactions on Industry Applications*, vol. 54, no. 5, pp. 5124–5133, 2018.

[17] S. Dong and Y. C. Chen, "Adjusting synchronverter dynamic response speed via damping correction loop," *IEEE Transactions on Energy Conversion*, vol. 32, no. 2, pp. 608–619, 2017.

[18] Y. Yu, S. K. Chaudhary, G. D. A. Tinajero, L. Xu, N. N. B. A. Bakar, J. C. Vasquez, and J. M. Guerrero, "A reference-feedforward-based damping method for virtual synchronous generator control," *IEEE Transactions on Power Electronics*, vol. 37, no. 7, pp. 7566–7571, 2022.

[19] Z. Shuai, W. Huang, Z. J. Shen, A. Luo, and Z. Tian, "Active power oscillation and suppression techniques between two parallel synchronverters during load fluctuations," *IEEE Transactions on Power Electronics*, vol. 35, no. 4, pp. 4127–4142, 2020.

[20] B. Yang, H. Li, S. Xu, H. Liu, and S. Lu, "Systematic methods to eliminate the transient circulating powers in the multi-vsgs system," *IEEE Transactions on Smart Grid*, vol. 15, no. 1, pp. 179–190, 2024.

[21] M. Li, P. Yu, W. Hu, Y. Wang, S. Shu, Z. Zhang, and F. Blaabjerg, "Phase feedforward damping control method for virtual synchronous generators," *IEEE Transactions on Power Electronics*, vol. 37, no. 8, pp. 9790–9806, 2022.

[22] J. Xiao, L. Wang, P. Bauer, and Z. Qin, "Virtual impedance control for load sharing and bus voltage quality improvement in low voltage ac microgrid," *IEEE Transactions on Smart Grid*, 2023.

[23] J. Xiao, L. Wang, Y. Wan, P. Bauer, and Z. Qin, "Distributed model predictive control based secondary control for power regulation in ac microgrids," *IEEE Transactions on Smart Grid*, 2024.

[24] J. Xiao, L. Wang, Z. Qin, and P. Bauer, "An adaptive cyber security scheme for ac micro-grids," in *2022 IEEE Energy Conversion Congress and Exposition (ECCE)*. IEEE, 2022, pp. 1–6.

[25] J. Xiao, L. Wang, P. Bauer, and Z. Qin, "Cyber secure-oriented communication network design for microgrids," in *2024 IEEE 15th International Symposium on Power Electronics for Distributed Generation Systems (PEDG)*. IEEE, 2024, pp. 1–6.

[26] M. H. Bollen and F. Hassan, *Integration of distributed generation in the power system*. John wiley & sons, 2011.